THE ASTROPHYSICAL JOURNAL LETTERS, 883:L44 (7pp), 2019 October 1 https://doi.org/10.3847/2041-8213/ab4138
© 2019. The American Astronomical Society. All rights reserved.

Discovery of an Mg II Changing-look Active Galactic Nucleus and Its Implications for a Unification Sequence of Changing-look Active Galactic Nuclei

Hengxiao Guo (郭恒潇)[1,2,9], Mouyuan Sun[3,4,5,9], Xin Liu[1,2], Tinggui Wang[3,4], Minzhi Kong[6,1,9], Shu Wang[7,8], Zhenfeng Sheng[3,4], and Zhicheng He[3,4]

[1] Department of Astronomy, University of Illinois at Urbana-Champaign, Urbana, IL 61801, USA; hengxiao@illinois.edu
[2] National Center for Supercomputing Applications, University of Illinois at Urbana-Champaign, Urbana, IL 61801, USA
[3] CAS Key Laboratory for Researches in Galaxies and Cosmology, University of Sciences and Technology of China, Hefei, Anhui 230026, People's Republic of China; ericsun@ustc.edu.cn
[4] School of Astronomy and Space Science, University of Science and Technology of China, Hefei 230026, People's Republic of China
[5] Department of Astronomy, Xiamen University, Xiamen, Fujian 361005, People's Republic of China
[6] Department of Physics, Hebei Normal University, No. 20 East of South 2nd Ring Road, Shijiazhuang 050024, People's Republic of China confucious_76@163.com
[7] Kavli Institute for Astronomy and Astrophysics, Peking University, Beijing 100871, People's Republic of China
[8] Department of Astronomy, School of Physics, Peking University, Beijing 100871, People's Republic of China

Received 2019 July 31; revised 2019 August 31; accepted 2019 September 4; published 2019 October 1

Abstract

Changing look (CL) is a rare phenomenon of active galactic nuclei (AGNs) that exhibit emerging or disappearing broad lines accompanied by continuum variations on astrophysically short timescales ($\lesssim$1 yr to a few decades). While previous studies have found Balmer-line (broad Hα and/or Hβ) CL AGNs, the broad Mg II line is persistent even in dim states. No unambiguous Mg II CL AGN has been reported to date. We perform a systematic search of Mg II CL AGNs using multi-epoch spectra of a special population of Mg II-emitters (characterized by strong broad Mg II emission with little evidence for AGNs from other normal indicators such as broad Hα and Hβ or blue power-law continua) from the Sloan Digital Sky Survey Data Release 14. We present the discovery of the first unambiguous case of a Mg II CL AGN, SDSS J152533.60+292012.1 (at redshift $z = 0.449$), which is turning off within rest-frame 286 days. The dramatic diminishing of Mg II equivalent width (from 110 ± 26 Å to being consistent with zero), together with little optical continuum variation ($\Delta V_{\max-\min} = 0.17 \pm 0.05$ mag) coevally over ~10 yr, rules out dust extinction or a tidal disruption event. Combined with previously known Hβ CL AGNs, we construct a sequence that represents different temporal stages of CL AGNs. This CL sequence is best explained by the photoionization model of Guo et al. In addition, we present two candidate turn-on Mg II CL AGNs and a sample of 361 Mg II-emitters for future Mg II CL AGN searches.

Unified Astronomy Thesaurus concepts: Active galaxies (17); Active galactic nuclei (16); Black hole physics (159)

1. Introduction

Changing look (CL) is a useful phenomenon to understand the physical structure of active galactic nuclei (AGNs) and a natural laboratory to explore the evolution between AGNs and normal galaxies. Despite the massive modern spectroscopic/photometric sky surveys, only dozens of Balmer-line CL AGNs have been discovered with type-transition timescales ranging from several months to decades (LaMassa et al. 2015; Ruan et al. 2016b; Runco et al. 2016; Runnoe et al. 2016), leading to a detection rate much smaller than 1% (MacLeod et al. 2016; Yang et al. 2018). The intrinsic nature of this rapid CL behavior was usually explained by dust reddening (e.g., Goodrich 1989; Tran et al. 1992), accretion rate change (e.g., LaMassa et al. 2015), or a tidal disruption event (TDE; Merloni et al. 2015). However, recent evidence (e.g., the polarization observation in Hutsemékers et al. 2017 and mid-infrared echo in Sheng et al. 2017) suggests that the variation of the accretion rate is likely to be the primary origin for CL AGNs, although the short transition timescale challenges the standard thin disk model (Shakura & Sunyaev 1973), which predicts a transition timescale of $\sim 10^4$ yr (MacLeod et al. 2016). In order to address the timescale problem, competing models, for example the magnetically elevated disk model (Dexter & Begelman 2019), and instabilities arising from magnetic torque near the event horizon (Ross et al. 2018) are proposed. On the other hand, repeating X-ray observations suggest that the CL phenomenon in supermassive black holes might be analogous to the structure of accretion flows in stellar-mass black holes (Ruan et al. 2019).

Previous observations have revealed the emerging or disappearing of broad Balmer lines (e.g., Hβ or Hα) in CL AGNs, whereas the broad Mg II is always persistent even in the dim state (MacLeod et al. 2016, 2019; Yang et al. 2018, 2019). To date, no unambiguous Mg II CL phenomenon has been reported.

On the other hand, Roig et al. (2014) discovered ~300 unusual broad Mg II-emitters. These sources show strong and broad Mg II line, but very weak emission in other normal indicators of AGN activity, such as Hα, Hβ, and near-ultraviolet power-law continuum. They considered these Mg II-emitters as a potentially new class of AGNs. However, we have argued that they are more likely to be the transition stage of CL AGNs (Guo et al. 2019, also see Section 3.3).

The difficulty of discovering Mg II CL might mainly be caused by the weak variability of the Mg II line (MacLeod et al. 2019; Yang et al. 2019). Previous reverberation-mapping programs encountered a similar situation, namely that the response of the Mg II line to continuum variation is often undetectable (e.g., Cackett et al. 2015) except for a few sources

[9] Corresponding author.

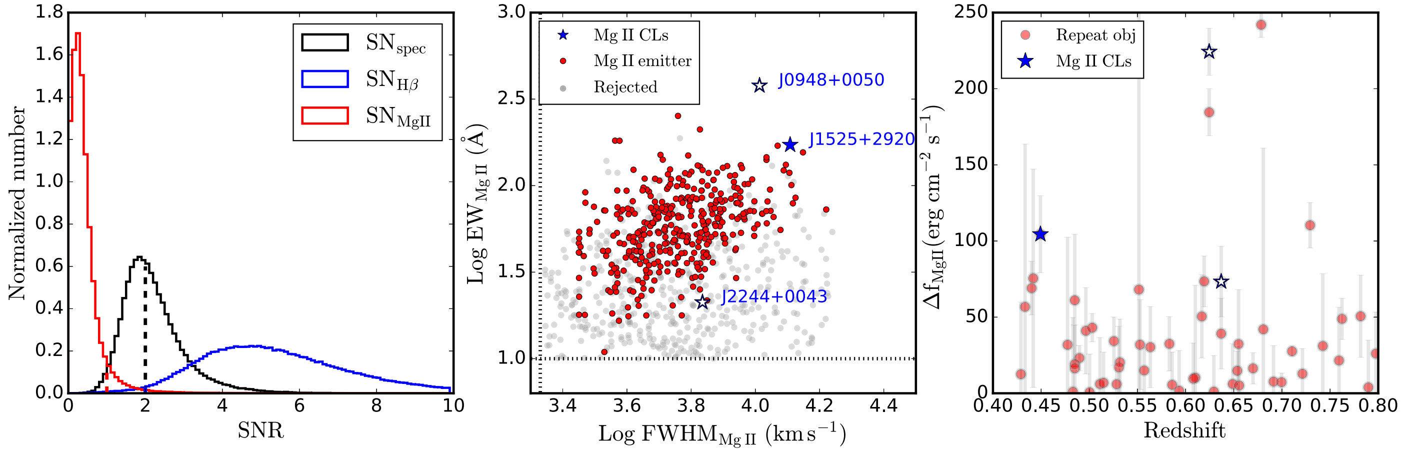

Figure 1. Left panel: distributions of the S/N for Mg II (red), Hβ (blue), and the whole spectrum (black). About 16,000 Mg II-emitter candidates with SN$_{Mg II} > 1$ and both SN$_{spec}$ and SN$_{H\beta} > 2$ are selected from the S/N cut. Middle panel: FWHM–equivalent width (EW) diagram of Mg II line. We compiled a sample of 361 Mg II-emitters (red dots) based on our criteria in Section 2.3. One unambiguous (filled blue star) and two tentative Mg II CL AGNs (empty blue stars) are marked. The gray dots are rejected candidates due to noise fitting or with significant broad Hβ component. Two black dotted lines are the lower limits of EW (>10 Å) and FWHM (>2000 km s^{-1}) to exclude the potential Type II AGNs and reduce the contamination from noise fitting. Right panel: Mg II line variability as a function of redshift. We find three Mg II CL AGNs out of 10 sources with significant Mg II variability ($>3\sigma$) in 52 Mg II-emitters with repeat observations.

(e.g., Clavel et al. 1991). Two possible mechanisms are proposed to explain the weak variability and the lack of response to continuum fluctuations: (1) geometric dilution that limits the relatively outer Mg II emitting region to getting only some of the scatter continuum emission (Sun et al. 2015), or (2) the intrinsic slow response of Mg II dominated by atomic physics and radiative transfer within the line-emitting clouds (Goad et al. 1993; Korista & Goad 2000; Guo et al. 2019).

In order to understand the phenomena of CL AGNs and Mg II-emitters, as well as the radiative mechanism of Mg II line, which is an important proxy of the black hole mass at quasar activity peak (i.e., $1 < z < 2$), we performed a series of works. In Guo et al. (2019), we first quantitatively compared the line-variability behaviors between Mg II and Balmer lines and demonstrated a good consistency of CL phenomenon with the photoionization models. In this Letter, we present the results of the first systematic search of Mg II CL AGNs by studying repeat spectra of Mg II-emitters from the Sloan Digital Sky Survey Data Release 14 (SDSS DR14). In particular, we present the discovery of the first unambiguous case of Mg II CL.

This Letter is organized as follows. In Section 2, we describe the data and sample selections for Mg II-emitters. In Section 3, we present an unambiguous Mg II CL, as well as two candidates for Mg II CL AGNs. Then we construct the observed CL sequence and discuss its implications. Finally, we draw our conclusion and discuss the future work in Section 4. Throughout this Letter, a cosmology with $H_0 = 70$ km s^{-1} Mpc^{-1}, $\Omega_m = 0.3$ and $\Omega_\Lambda = 0.7$ was adopted.

2. Data and Sample Selection

2.1. SDSS Spectrum

All the spectra in this work are obtained from the public SDSS DR14 database (Abolfathi et al. 2018), which covers 14,555 deg^2. A benefit of its ~20 yr cumulative data is the fact that extensive multi-epoch spectra are quite suitable for investigating the AGN spectral variability. The multi-epoch spectroscopic observations are mainly from three parts: (1) the overlapped survey areas between adjacent plates; (2) dedicated programs, e.g., the Time Domain Spectroscopic Survey (Ruan et al. 2016a) and SDSS reverberation mapping (Shen et al. 2015); (3) re-observed plates due to insufficient signal-to-noise ratio (S/N). The spectral wavelength coverage for SDSS I&II (SDSS III) is 3800–9200 (3600–10400) Å with spectral resolution $R \sim 1850$–2200, and the five-band *ugriz* magnitudes have typical errors of about 0.03 mag in depth to 22.0, 22.2, 22.2, 21.3, 20.5 mag (Abazajian et al. 2009).

2.2. Catalina Sky Survey (CSS) Light Curve

Although the optical light curves are not used to select Mg II CL AGNs in Section 2.3, they are still useful for understanding the origins of the CL behavior. CSS (Drake et al. 2009) repeatedly covered 26,000 deg^2 on the sky using a 0.7 m Schmidt telescope with a wide field of view of 8.1 deg^2. The photometric data were unfiltered and calibrated to *V*-band magnitude, to a depth of ~20 mag.

2.3. Sample Selection of Mg II-emitters

Previous observations of CL AGNs indicate that the so-called Mg II-emitters are likely to be the faint states of Hβ CL AGNs (MacLeod et al. 2016; Yang et al. 2018; MacLeod et al. 2019). In order to search both Mg II and Hβ CL AGNs, we define the Mg II-emitters as those with prominent broad Mg II but no broad Hβ component (FWHM$_{H\beta} < 1000$ km s^{-1}), similar to Roig et al. (2014). The advantage of this approach is being able to discover both Mg II and Hβ CL AGNs based on the multi-epoch spectra when AGNs turn off or on. Compared with the widely used variability-color selection (MacLeod et al. 2016, 2019; Sheng et al. 2017; Yang et al. 2018), our method servers as a tailored approach for searching Mg II CL AGNs at low luminosity end, as all of the Mg II-emitters are very faint (see below).

We start with all spectra (4.8 million) in SDSS DR14 database (Abolfathi et al. 2018). Following are the selection criteria for Mg II-emitter candidates.

1. Redshift: $0.4 < z < 0.8$, zWarning = 0.
2. Class = "QSO" or "GALAXY."
3. Mg II flux > 0, and (FWHM$_{H\beta} < 1000$ km s^{-1} or Hβ flux < 0).
4. SN$_{spe} > 2$, SN$_{H\beta} > 2$ and SN$_{Mg II} > 1$.

Table 1
Information for Mg II CL AGNs (Hereafter J1525+2920, J0948+0050 and J2244+0043) from SDSS

SDSS Designation (1)	Redshift (2)	g-band (mag) (3)	Log M_{BH} ($M_{\odot}$) (4)	λ_{Edd} (10^{-3}) (5)	Type (6)	Plate (7)	MJD (8)	Fiber (9)	State (10)
J152533.60+292012.1	0.449	21.62 ± 0.11	8.0 ± 0.1	3.3	turn off	3879	55244	103	bright
…						3963	55659	731	faint
…						4721	55709	723	faint
J094810.92+005057.8	0.624	21.59 ± 0.09	7.4 ± 0.1	16.2	turn on	480	51989	99	faint
…						3827	55565	699	bright
J224448.72+004347.1	0.637	21.10 ± 0.04	7.8 ± 0.2	3.7	turn on	675	52590	489	faint
…						4204	55470	982	bright

Note. Columns include the object name, redshift, g-band magnitude, Mg II-based black hole mass and 1σ statistical error, averaged Eddington ratio of bright and faint states, transition type, plate ID, MJD, fiber ID, and the luminosity state. Note that J0948+0050 was also collected in Mg II-emitter catalog of Roig et al. (2014).

To include the Mg II line, Hβ–[O III] complex of AGNs, and simultaneously avoid the emission lines that are too close to the spectral edges resulting in low S/Ns, Criteria 1 and 2 are applied. In addition, Criterion 3 ensures that the Mg II (Hβ) is emission line (narrow emission line or absorption line) based on the measurements from SDSS automatic pipeline (Bolton et al. 2012). As shown in left panel of Figure 1, the S/Ns of continuum and lines (Criterion 4) are needed to ensure the spectral qualities of the candidates. We note that all these candidates are very faint with a typical flux density of 10^{-17} erg cm^{-2} s^{-1} Å^{-1} at 3000 Å, thus the S/Ns are lower than the typical values of ordinary quasars (e.g., 5 ~ 10 in Shen et al. 2011). These four criteria yield ~16,000 Mg II-emitter candidates.

Then we use PyQSOFit[10] (Guo et al. 2018; Shen et al. 2019) to perform the local fit for the Mg II region ([2700, 2900] Å) with a power-law continuum, iron template and up to three Gaussian profiles to extract the line properties. To exclude the potential Type II AGNs with narrow Mg II doublets and also alleviate the noise fitting, we select the candidates with

1. $2000\ \mathrm{km\ s^{-1}} < \mathrm{FWHM_{Mg\,II}} < 20000\ \mathrm{km\ s^{-1}}$ and $\mathrm{EW_{Mg\,II}} > 10$ Å.

This leaves ~800 objects (red and gray dots), shown in the middle panel of Figure 1.

Next, we visually inspect each spectrum to confirm that the spectral fitting for Mg II line and the measurements of Hβ line from SDSS automatic pipeline are reasonable. About half of ~800 objects, usually located in the lower-right portion of FWHM–EW diagram, were excluded because of the extremely week broad Mg II line blending with the continuum, which can significantly affect the spectral decomposition. Another ~50 objects showing significant broad Hβ components[11] are also excluded, which are usually with large $\mathrm{EW_{Mg\,II}}$ located in the upper portion of the FWHM–EW diagram. This process leaves us a sample of 361 (with a detection rate of ~0.02% in ~2 million galaxies/quasars) unique Mg II-emitters,[12] including 52 objects with multi-epoch observations. Their spectra also usually show significant galactic features, e.g., strong absorption lines (e.g., Ca H+K), 4000 Å break and weak power-law continuum.

Finally, we refit the brightest and faintest epochs of these 52 Mg II-emitters, and find 10 objects with significant Mg II variability ($>3\sigma$) in the right panel of Figure 1. Rejecting seven ordinary sources due to normal broad Mg II variation without CL behavior, this leaves three Mg II CL AGNs (see Figures 1–3 and Table 1), i.e., a detection rate of ~0.001% (3/52 × 0.02%) based on Mg II-emitters, which is consistent with that of Hβ CL AGNs in Yang et al. (2018). We also discovered new Hβ CL AGNs, which will be shown in a future paper.

3. Results and Discussion

3.1. Discovery of the First Mg II CL AGN

Figure 2 shows an unambiguous turn-off Mg II CL AGN (J1525+2920) at $z = 0.449$. This object was first selected as a Mg II-emitter in the bright state by our work, which was targeted as a luminous red galaxy by SDSS. J1525+2920 shows a dramatic change in Mg II EW, i.e., $\mathrm{EW_{Mg\,II}} = 110 \pm 26$ Å to 0 (or $\Delta f_{\mathrm{Mg\,II}} = 103 \pm 25$ erg cm^{-2} s^{-1} at 4σ level), with a factor of 2 continuum variation blueward of rest frame 4000 Å, which rules out the dust-reddening scenario for CL behavior as this model expects a constant line $\mathrm{EW_{Mg\,II}}$. Moreover, the accompanied disappearing of helium and iron lines at 3191 and 3581 Å, as typical features of CL AGNs and TDEs (Brown et al. 2016; Yan et al. 2019), further supports that this is a genuine Mg II CL event rather than a false alarm due to the calibration problem.[13] The self-consistence of two faint epochs[14] also suggests that the SDSS flux calibration is robust for this object. The residual spectrum (bright-faint) is well fitted by a power-law continuum $f_\lambda = \lambda^{-1.24\pm0.05}$, which may indicate a possible AGN origin of the varying component.[15] Its rest-fame transition timescale is less than 286 days, which is consistent with other normal Hβ CL AGNs (MacLeod et al. 2016; Yang et al. 2018).

By convolving with the SDSS filters, this source shows the variations in g- and r-band are 0.54 ± 0.02 mag and 0.1 ± 0.01 mag, respectively, which would be missed by

[10] A public python code for quasar spectral fitting, see https://github.com/legolason/PyQSOFit.

[11] For these sources, the SDSS automatic pipeline fitting results are biased; therefore, we refit their Hβ–[O III] complex for further confirmation.

[12] The Mg II-emitter catalog is available here: https://github.com/legolason/MgII-emitter-catalog. Through privately obtained Mg II-emitter catalog from Roig et al. (2014), we found that the overlaps between two catalog are less than 10% due to the different selection criteria.

[13] We checked that the quality of the plates is good, and that other objects in these plates are normal.

[14] See all spectra here: http://skyserver.sdss.org/ with R.A., decl. = (15:25:33.60, +29:20:12.12).

[15] The typical optical slope of AGN is $f_\lambda = \lambda^{-1.54\pm0.49}$, see Guo & Gu (2016) for details.

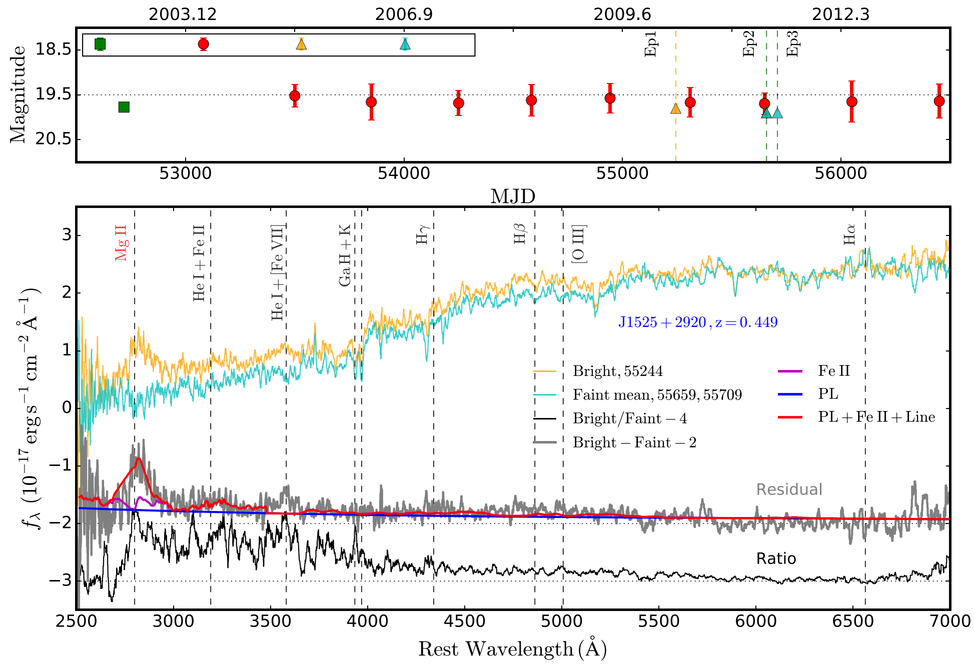

Figure 2. Unambiguous turn-off CL phenomenon of J1525+2920. The bottom panel shows the bright state (orange) and faint state (green, the mean of two faint epochs to improve the S/Ns) with box-car smoothing of 10 pixels for clarity. The broad Mg II line disappears accompanied by helium and iron lines (3191 and 3581 Å) with fading continuum in 286 days in the rest frame. The residuals (gray) are well fitted by a model (red) consisting of a power law (blue), iron template (magenta), and one Gaussian profile. The spectral ratio (black) of the bright and faint states shows that the relatively larger variability in the blueward. The dotted lines under the spectral ratio and the residuals are added to guide the eye, and the dashed lines mark the prominent lines in ultraviolet (UV)/optical bands. The top panel presents the seasonally averaged CSS light curve, together with photometries from three SDSS spectra and SDSS-*r*. Only small variations (0.17 ± 0.05 mag) can be detected on a timescale of $\sim$10 yr. The corresponding spectra are marked with dashed orange/green lines.

conventional variability selections (e.g., $\Delta g > 1$ mag, MacLeod et al. 2016; Rumbaugh et al. 2018).

The seasonally averaged CSS light curve in the upper panel of Figure 2, together with these *r*-band synthetic magnitudes obtained from three spectra and SDSS-*r*, indicates a weak variability ($\Delta V_{\rm max-min} = 0.17 \pm 0.05$ mag) over 10 yr. This strongly disfavors the TDE scenario, which typically exhibits a rapid raising phase with several magnitudes and a slow decay by $\sim t^{-5/3}$ within at most several years (Rees 1988; Evans & Kochanek 1989), as well as some temporal supernova-driven broad emission lines (Simmonds et al. 2016). The slight difference in the photometric systems of SDSS and CSS can be safely ignored for our purposes.

Given the $\mathrm{FWHM}_{\rm Mg\,II} = 12{,}700 \pm 300$ km s^{-1}, we estimate the black hole mass of $M_{\rm BH} = 10^{8.0\pm0.1}\ M_\odot$ (1σ statistical error) according to Shen et al. (2011), and hence the averaged Eddington ratio $\lambda_{\rm Edd} = L_{\rm bol,(bright+faint)/2}/L_{\rm Edd} \sim 3.3 \times 10^{-3}$, where $L_{\rm Edd} = 1.26 \times 10^{38} M_{\rm BH}/M_\odot$ erg s^{-1}. Here we emphasize that the Mg II line usually does not follow the breathing mode (Shen 2013; Yang et al. 2019); i.e., the line width may not change with continuum variation, and whether there is an intrinsic *R*–*L* is still unclear. Thus, the black hole mass based on Mg II bears a larger uncertainty compared to Hβ.

3.2. Two Turn-on Mg II CL Candidates

Figure 3 exhibits two tentative turn-on Mg II CL AGNs, and both of their bright states are selected as Mg II-emitters. Together with J1525+2920, we find that all three Mg II transitions occurred when $f_{3000\,\text{Å}}$ is below 10^{-17} erg cm^{-2} s^{-1} Å^{-1} (or $L_{3000\,\text{Å}} < 10^{43.5}$ erg s^{-1}), which is much fainter than normal Hβ CL AGNs (MacLeod et al. 2016; Yang et al. 2018).

J0948+0050. The Mg II variability in this object is very significant with $\Delta f_{\rm Mg\,II} = 224 \pm 18$ erg cm^{-2} s^{-1} ($>5\sigma$). However, in the faint state, there is still a small remnant of the broad Mg II. The light curve shows a strong variability of $\sim$1 mag over a timescale of $\sim$10 yr.

J2244+0043. The Mg II variability in this object is relatively weak with $\Delta f_{\rm Mg\,II} = 73 \pm 23$ erg cm^{-2} s^{-1} ($>3\sigma$). The $\mathrm{EW}_{\rm Mg\,II} = 18 \pm 7$ Å is also small, which almost reaches the lower EW boundary of Mg II-emitters in Figure 1. The residuals of bright and faint epochs show an insignificant broad Hβ line. The light curve indicates that it varies $\sim$0.5 mag over a timescale of $\sim$10 yr.

Due to the lack of obvious accompanied transitions (e.g., iron and helium lines) and verification from multi-epoch spectra, together with the concerns above, we classified them as tentative Mg II CL AGNs. If they keep brightening further, we would expect the appearance of a broad Hβ component.

3.3. A CL Sequence

Recently, Guo et al. (2019) demonstrated that the dramatic changes in broad Hα/Hβ emission in the observationally rare CL quasars are fully consistent with their photoionization model, and the theoretical CL sequence predicted by their model provides natural explanations for the persistence of broad Mg II in CL quasars defined on Hα/Hβ and the rare population of broad Mg II-emitters (see their Figure 8).

Here we recovered an observed CL sequence with three real CL AGNs at different temporal evolution stages to confirm their prediction of the photoionization model. In Figure 4, two known multi-epoch Hβ CL AGNs (J141324.27+530526.9, gray lines, $z = 0.457$ in Dexter & Begelman 2019 and J022556.07 +003026.7, green lines, $z = 0.504$ in MacLeod et al. 2016), together with our Mg II CL AGN (J1525+2920, red lines,

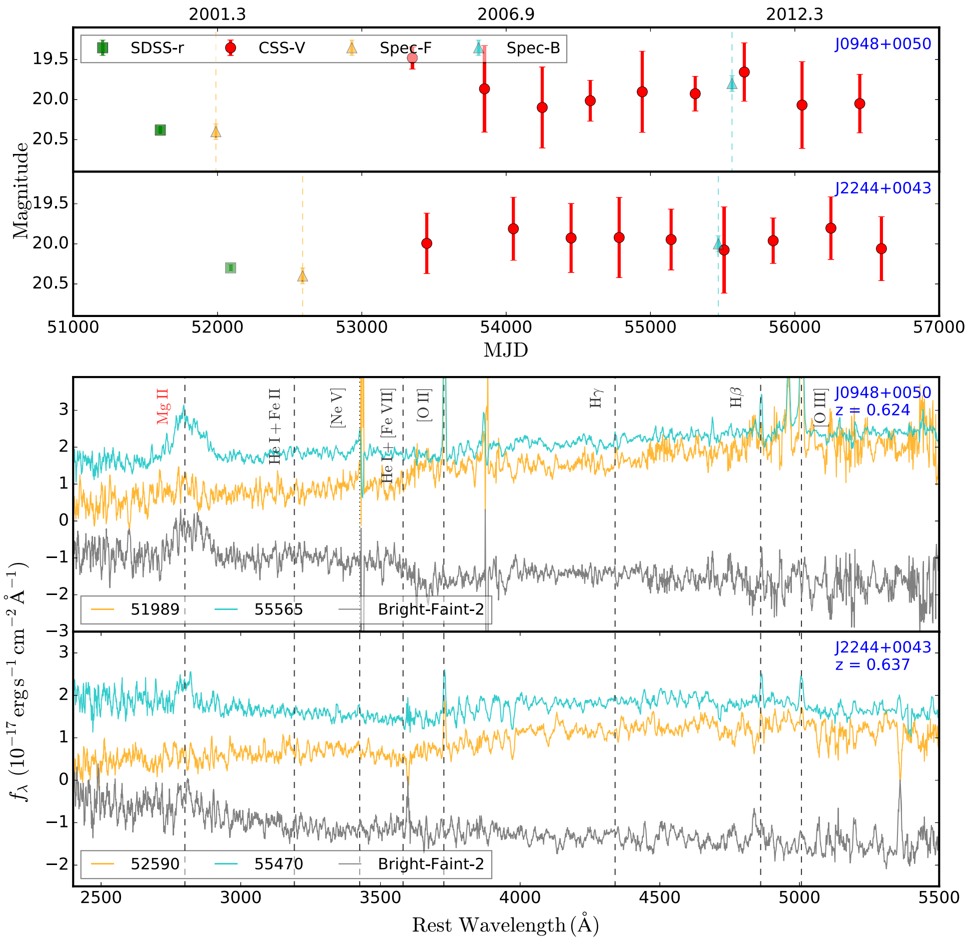

Figure 3. Two tentative turn-on Mg II CL AGNs. Bottom panel: both bright states (green) are selected as Mg II-emitters. With continuum turned on, J0948+0050 presents a strong broad Mg II within 2202 rest-frame days, while J2244+0043 shows a weak broad Mg II and disappearance of the absorption features of Balmer lines within 1759 rest-frame days. For clarity, all the spectra are smoothed with a box-car of 10 pixels. Top panel: the multi-survey light curves show the maximum variabilities of ∼1 mag and ∼0.5 mag for J0948+0050 and J2244+0043, respectively.

$z = 0.449$), are selected to construct the observed CL sequence in bright, intermediate, and faint stages. The Mg II lines share a similar profile for the faintest epoch of intermediate Hβ CL AGN and the brightest epoch of the Mg II CL AGN, as well as the Mg II and Balmer lines in between the bright and intermediate CL AGNs. This allows for temporal stages in three different CL AGNs to link together, mimicking the variability evolution in a CL object and compensating for the lack of multi-epoch spectroscopy across the full sequence in a single object. Although, the exact broad line width may be different or slightly affected by non-response effect in Mg II (Guo et al. 2019), it would be trivial for demonstrating the concept of broad line disappearance.

As shown in Figure 4, when the broad Balmer lines almost disappear (e.g., become undetectable), the broad Mg II emission is still substantial. While the continuum luminosity continues to drop, the broad Mg II eventually becomes too weak to be detectable. In this sequence, some faint epochs of the intermediate Hβ CL AGN and brightest epoch of Mg II CL AGN are the so-called Mg II-emitters. Thus, we speculate that the Mg II-emitter is more likely to be the transition quasar population, where the quasar continuum and broad Balmer-line flux had recently dropped by a large factor but the broad Mg II flux is still detectable on top of the stellar continuum. We also notice that the Mg II line always disappears later than Hα because Mg II has both less variability and suffers less contamination from the host galaxy. All these features are consistent with the theoretical CL sequence predicated by the photoionization model in Guo et al. (2019).

4. Conclusion and Future Work

We have presented a systematic study of the spectroscopic variability of a sample of Mg II-emitters using multi-epoch spectra from the SDSS DR14. We have discovered the first unambiguous case of a Mg II CL AGN, which is turning off within 286 days in the rest frame, as well as two candidate turn-on Mg II CL AGNs. Together with two previously known Hβ CL AGNs, we have constructed a unification sequence that represents different temporal stages of CL AGNs incorporating both broad Balmer-line and broad Mg II CL AGNs. We conclude that this CL AGN unification sequence is best explained by the photoionization model suggested by Guo et al. (2019), which indicates that most CL AGNs can be explained by the photoionization model. In this AGN CL sequence unification picture, Mg II-emitters (Roig et al. 2014) are naturally explained as an intermediate stage of CL AGNs rather than a new AGN population.

We have also assembled a sample of 361 unique Mg II-emitters, including 52 objects with multi-epoch spectra. They are useful for future searches of Mg II CL AGNs with dedicated spectroscopic time-domain surveys (e.g., SDSS-V; Kollmeier et al. 2017; The MSE Science Team et al. 2019). With ∼6% (3/52) Mg II CL AGNs in Mg II-emitters without accounting

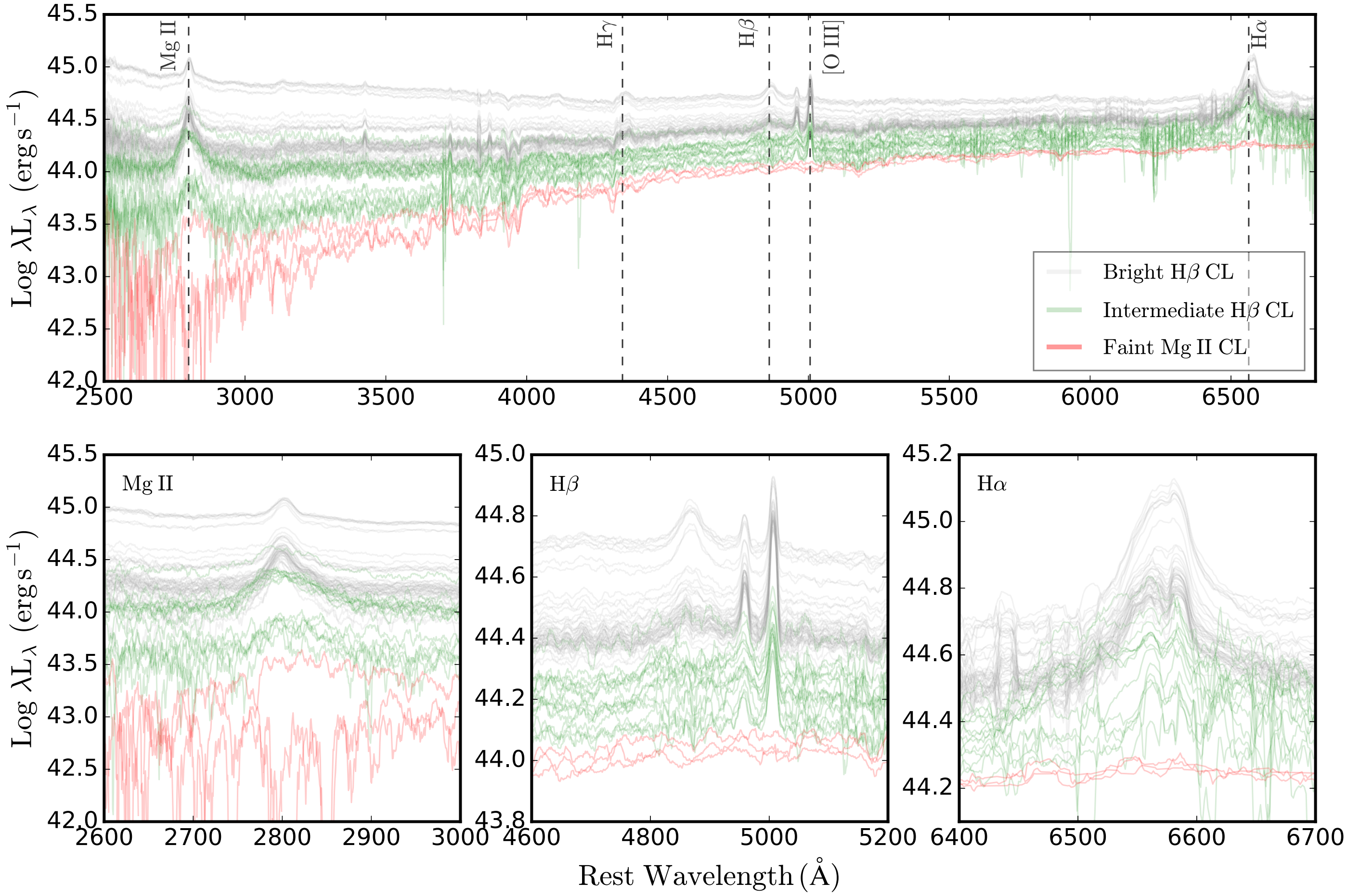

Figure 4. CL sequence. This compilation, presented sequentially with continuum luminosity decreasing, provides a representation of how the quasar type, signaled by the varying strength of the different emission lines (i.e., Mg II and Balmer lines), may transition with luminosity. The sequence is constructed using three known CL objects from bright (SDSS J141324.27+530526.9, gray, $z = 0.457$ in Dexter & Begelman 2019), intermediate (SDSS J022556.07+003026.7, green, $z = 0.504$, in MacLeod et al. 2016), and faint states (J1525+2920, red, $z = 0.449$) at similar redshifts. All the multi-epoch spectra are obtained from the SDSS database.

for selection incompleteness and selection biases, we would expect to discover about 20 Mg II CL AGNs, assuming that the full sample is monitored over a decade with an average cadence of ∼a year. A significantly larger sample of CL AGNs will help put our results on firm statistical ground.

We thank our referee for a prompt and constructive report that helped significantly improve this Letter. We thank Y. Shen for helpful discussions. M.Y.S. acknowledges the support from NSFC-11603022. M.Z.K. is supported by Astronomical Union Foundation under grant No. U1831126 and Natural Science Foundation of Hebei Province No. A2019205100.

Funding for the Sloan Digital Sky Survey IV has been provided by the Alfred P. Sloan Foundation, the U.S. Department of Energy Office of Science, and the Participating Institutions. SDSS-IV acknowledges support and resources from the Center for High-Performance Computing at the University of Utah. The SDSS website is www.sdss.org. SDSS-IV is managed by the Astrophysical Research Consortium for the Participating Institutions of the SDSS Collaboration including the Brazilian Participation Group, the Carnegie Institution for Science, Carnegie Mellon University, the Chilean Participation Group, the French Participation Group, Harvard-Smithsonian Center for Astrophysics, Instituto de Astrofísica de Canarias, The Johns Hopkins University, Kavli Institute for the Physics and Mathematics of the Universe (IPMU)/University of Tokyo, Lawrence Berkeley National Laboratory, Leibniz Institut für Astrophysik Potsdam (AIP), Max-Planck-Institut für Astronomie (MPIA Heidelberg), Max-Planck-Institut für Astrophysik (MPA Garching), Max-Planck-Institut für Extraterrestrische Physik (MPE), National Astronomical Observatories of China, New Mexico State University, New York University, University of Notre Dame, Observatário Nacional/MCTI, The Ohio State University, Pennsylvania State University, Shanghai Astronomical Observatory, United Kingdom Participation Group, Universidad Nacional Autónoma de México, University of Arizona, University of Colorado Boulder, University of Oxford, University of Portsmouth, University of Utah, University of Virginia, University of Washington, University of Wisconsin, Vanderbilt University, and Yale University.

The CSS survey is funded by the National Aeronautics and Space Administration under grant No. NNG05GF22G issued through the Science Mission Directorate Near-Earth Objects Observations Program.

ORCID iDs

Hengxiao Guo (郭恒潇) https://orcid.org/0000-0001-8416-7059
Mouyuan Sun https://orcid.org/0000-0002-0771-2153
Xin Liu https://orcid.org/0000-0003-0049-5210

Tinggui Wang https://orcid.org/0000-0002-1517-6792
Zhenfeng Sheng https://orcid.org/0000-0001-6938-8670

References

Abazajian, K. N., Adelman-McCarthy, J. K., Agüeros, M. A., et al. 2009, ApJS, 182, 543
Abolfathi, B., Aguado, D. S., Aguilar, G., et al. 2018, ApJS, 235, 42
Bolton, A. S., Schlegel, D. J., Aubourg, É., et al. 2012, AJ, 144, 144
Brown, J. S., Shappee, B. J., Holoien, T. W. S., et al. 2016, MNRAS, 462, 3993
Cackett, E. M., Gültekin, K., Bentz, M. C., et al. 2015, ApJ, 810, 86
Clavel, J., Reichert, G. A., Alloin, D., et al. 1991, ApJ, 366, 64
Dexter, J., & Begelman, M. C. 2019, MNRAS, 483, L17
Drake, A. J., Djorgovski, S. G., Mahabal, A., et al. 2009, ApJ, 696, 870
Evans, C. R., & Kochanek, C. S. 1989, ApJL, 346, L13
Goad, M. R., O'Brien, P. T., & Gondhalekar, P. M. 1993, MNRAS, 263, 149
Goodrich, R. W. 1989, ApJ, 340, 190
Guo, H., & Gu, M. 2016, ApJ, 822, 26
Guo, H., Shen, Y., He, Z., et al. 2019, arXiv:1907.06669
Guo, H., Shen, Y., & Wang, S. 2018, PyQSOFit: Python code to fit the spectrum of quasars version 1.0, Astrophysics Source Code Library, ascl:1809.008
Hutsemékers, D., Agís González, B., Sluse, D., Ramos Almeida, C., & Acosta Pulido, J. A. 2017, A&A, 604, L3
Kollmeier, J. A., Zasowski, G., Rix, H.-W., et al. 2017, arXiv:1711.03234
Korista, K. T., & Goad, M. R. 2000, ApJ, 536, 284
LaMassa, S. M., Cales, S., Moran, E. C., et al. 2015, ApJ, 800, 144
MacLeod, C. L., Green, P. J., Anderson, S. F., et al. 2019, ApJ, 874, 8
MacLeod, C. L., Ross, N. P., Lawrence, A., et al. 2016, MNRAS, 457, 389
Merloni, A., Dwelly, T., Salvato, M., et al. 2015, MNRAS, 452, 69
Rees, M. J. 1988, Natur, 333, 523
Roig, B., Blanton, M. R., & Ross, N. P. 2014, ApJ, 781, 72
Ross, N. P., Ford, K. E. S., Graham, M., et al. 2018, MNRAS, 480, 4468
Ruan, J. J., Anderson, S. F., Cales, S. L., et al. 2016a, ApJ, 826, 188
Ruan, J. J., Anderson, S. F., Eracleous, M., et al. 2019, arXiv:1903.02553
Ruan, J. J., Anderson, S. F., Green, P. J., et al. 2016b, ApJ, 825, 137
Rumbaugh, N., Shen, Y., Morganson, E., et al. 2018, ApJ, 854, 160
Runco, J. N., Cosens, M., Bennert, V. N., et al. 2016, ApJ, 821, 33
Runnoe, J. C., Cales, S., Ruan, J. J., et al. 2016, MNRAS, 455, 1691
Shakura, N. I., & Sunyaev, R. A. 1973, A&A, 500, 33
Shen, Y. 2013, BASI, 41, 61
Shen, Y., Brandt, W. N., Dawson, K. S., et al. 2015, ApJS, 216, 4
Shen, Y., Hall, P. B., Horne, K., et al. 2019, ApJS, 241, 34
Shen, Y., Richards, G. T., Strauss, M. A., et al. 2011, ApJS, 194, 45
Sheng, Z., Wang, T., Jiang, N., et al. 2017, ApJL, 846, L7
Simmonds, C., Bauer, F. E., Thuan, T. X., et al. 2016, A&A, 596, A64
Sun, M., Trump, J. R., Shen, Y., et al. 2015, ApJ, 811, 42
The MSE Science Team, Babusiaux, C., Bergemann, M., et al. 2019, arXiv:1904.04907
Tran, H. D., Osterbrock, D. E., & Martel, A. 1992, AJ, 104, 2072
Yan, L., Wang, T., Jiang, N., et al. 2019, ApJ, 874, 44
Yang, Q., Shen, Y., Chen, Y.-C., et al. 2019, arXiv:1904.10912
Yang, Q., Wu, X.-B., Fan, X., et al. 2018, ApJ, 862, 109